University of Nevada, Reno

Statistics of Ground Motions in a Foam Rubber Model of a Strike-Slip Fault

A thesis submitted in partial fulfillment of the requirements for the degree of
Master of Science in Geophysics

by

Kevin M. McBean

Dr. John G. Anderson/Thesis Advisor

May, 2015

UNIVERSITY OF NEVADA RENO **THE GRADUATE SCHOOL**

We recommend that the thesis
prepared under our supervision by

KEVIN M. McBEAN

entitled

Statistics of Ground Motions in a Foam Rubber Model of a Strike-Slip Fault

be accepted in partial fulfillment of the
requirements for the degree of

MASTER OF SCIENCE

John G. Anderson, Ph.D., Advisor

William Hammond, Ph.D., Committee Member

Edward Keppelmann, Ph.D., Graduate School Representative

David W. Zeh, Ph.D., Dean, Graduate School

May 2015

Abstract

The peak acceleration and velocity from 5058 ruptures of a foam rubber stick-slip model are not distributed according to a lognormal probability distribution function. PGA and PGV values are decomposed using the method of Anderson and Uchiyama (2011). The statistically significant deviations from the lognormal distribution occur near the peak of the distribution. In some cases, high-amplitude tails differ by a much greater ratio, but the statistical significance of this effect is low. This result is true of both raw data and data adjusted for site and magnitude. Event terms are also not lognormal, but can be modeled as a sum of three or four lognormal subdistributions, which possibly represent different preferred rupture initiation points rather than a uniform distribution of initiation points. The event term subdistributions with highest median values have small standard deviations, so if shapes of this nature were used in ground motion prediction equations (GMPEs) during a probabilistic seismic hazard analysis, the effect of the long tail of the lognormal distribution in controlling the hazard would be weakened considerably. Static stress drop was recorded for each event, and event terms for PGA and PGV are well correlated with static stress drop. Unlike NGAW2 GMPEs, residual variances for the foam model are dominated by variability in the source slip function, rather than the path and site effects. This difference in the variance budget results from the way in which the source and site residuals are defined in this study; the source uncertainty includes variation in the rupture size (magnitude) and location, along with deviations in distance and path. We do not know if these results apply to earthquakes but we do think tests of repeating stick-slip events in a physical system are useful to expand the set of credible hypotheses regarding possible behavior modes of earthquake faults.

Table of Contents

Contents

List of Tables

List of Tables

List of Figures

List of Figures

Part I

Introduction

The field of earthquake seismology is inherently data-starved. There are several reasons for this: return periods for large earthquakes are very long - on the order of 100 to 10,000 years; in addition, modern instrumental recordings of earthquakes only exist for the past eighty years, and spatial coverage of seismometers in seismically active regions is not very dense. As a result, when damaging earthquakes occur, they are often not very well recorded and produce datasets too small for robust statistical analysis. These small datasets limit the accuracy and precision of ground motion prediction models, which are an essential element of probabilistic seismic hazard analysis (PSHA), the current preferred method used to assess seismic risk (Abrahamson, 2006).

When ground motion prediction models in the form of ground motion prediction equations (GMPEs) are developed, they are generated using the limited ground motion datasets from instrumental recordings of past earthquakes. After the peak ground motion data are adjusted for magnitude, distance and site conditions, the data are assumed to be lognormally distributed; Restrepo-Velez and Bommer (2003) state that, "The assumption of lognormal distributions for the peak values of the strong-motion parameters is widely accepted." The reason for assuming a lognormal distribution begins with the observation that the sum of many random variables tends toward a normal distribution. Ground motions generated by earthquakes have contributions from many terms, including the earthquake faulting source, the path from the source to the site, and the effect of the site conditions. In the frequency domain, the ground motions from an earthquake are considered to be the product of each of these terms. If each of the terms is a random variable, then their sum in log space would tend toward a normal distribution; a normal distribution in log space is a lognormal distribution.

The output of certain GMPEs, given as a mean and standard deviation, are used along with an assumption of a lognormal distribution around the GMPE mean in the development of the national seismic hazard maps (e.g. Petersen et al., 2014) developed by the United States Geological Survey (USGS). These maps are generated by setting up a grid for the entire country, calculating a hazard curve for each node of the grid, using the hazard curves to determine a value for a ground motion parameter at a given target hazard level, and contouring those ground motion values. There are different maps created for prescribed hazard levels and ground motion parameters. The hazard curve

(for each grid node) is calculated using the hazard integral:

$$\lambda_C(a_m \geq a) = \int_{space} \int_{M_{min}}^{M_{max}} n(\mathbf{x}, M)\Phi(a_m \geq a \mid \hat{Y}, \sigma_T) dM d\mathbf{x},$$

where $\lambda_C(a_m \geq a)$ is the annual exceedance rate, $n(\mathbf{x}, M)$ is the seismicity model, and $\Phi(a_m \geq a \mid \hat{Y}, \sigma_T)$ is the GMPE. In this equation, a is used to denote acceleration; however, any other ground motion parameter can also be used. Thus, the term $\lambda_C(a_m \geq a)$ is the number of earthquakes per year where the peak acceleration exceeds the given acceleration a. The seismicity model $n(\mathbf{x}, M)$ gives the annual number of events with a magnitude M at a location $\mathbf{x}$. This model is developed by considering the faults near the site, their magnitudes and rates of seismicity along with a smoothed background seismicity to account for unknown faults that may contribute to the seismicity. The GMPE $\Phi(a_m \geq a \mid \hat{Y}, \sigma_T)$ gives the probability of exceeding an acceleration a given the magnitude, distance, and other input parameters. Its output is $\hat{Y}$ and σ_T, where $\hat{Y}$ is the mean prediction of the ground motion parameter (PGA in this case) and σ_T is the standard deviation of $\hat{Y}$. In other words, the GMPE outputs a distribution of the ground motion parameter values, and the distribution is assumed to be lognormal (e.g. Bommer et al., 2004). Therefore, the hazard integral calculates the probability of exceeding the ground motion parameter by considering the distribution of ground motions around the mean of that parameter.

The appropriateness of using a lognormal distribution for peak ground motions has not been extensively studied. Part of the reason for this is that the relatively small sample sizes of earthquake-induced ground motion recordings do not allow for a robust analysis of distributions. The few studies that have been performed have given mixed results. Two studies (Ambraseys et al., 2005 and Cauzzi and Faccioli, 2008) looked at the effectiveness of using a logarithmic transformation on earthquake-induced ground motions at several spectral periods. Both studies found that the logarithmic transformation was not appropriate for some periods, but it was at neighboring periods, which led the researchers to conclude that the use of the transformation was justified. In contrast, a different study (Douglas and Smit, 2001) used the same method on a different dataset and concluded that the logarithmic transformation was appropriate for all spectral periods. Restrepo-Velez and Bommer (2003) investigated the distribution of recorded ground motions from a European database as well as from GMPE residuals, which are the differences in logarithms from the prediction. They found that the ground motions and the residuals are lognormally distributed except at the tails of

the distribution. Yamada et al. (2009) studied the distribution of peak ground motions of large earthquakes recorded near the source and found that peak ground accelerations are consistent with a lognormal distribution, and peak ground displacements are lognormally distributed at a given magnitude.

When statistical analyses are performed using the small datasets from instrumental records, the results include a large amount of uncertainty in the system both in the form of natural aleatory variability and in the form of epistemic uncertainty from our lack of knowledge about the components of the system. Consequently, the statistical significance of the analysis is often limited due to the significant amount of uncertainty.

To supplement the knowledge gained from analyses of earthquake records, experimental models, either physical or numerical in nature, can be used to produce large datasets. In many physical models, the stick-slip mechanism of earthquakes is recreated using two surfaces that are initially statically bound together by friction until the driving stress accumulated at the interface exceeds the strength of the frictional force, and slip occurs. A model that generates repeated stick-slip ruptures in a material with properties similar to the earth's crust can provide datasets suitable for detailed statistical analysis and with a higher level of significance than when small datasets from earthquakes are used. One such suitable modeling material is foam rubber. Although the density and strain rates of foam rubber are different from those occurring in the earth, foam rubber has a similar Poisson's ratio and rupture velocity to crustal rock at seismogenic depths. This allows for rupture and wave propagation properties in the model to resemble those found in crustal rock.

To investigate the nature of stick-slip ruptures, by generating a large dataset from many ruptures, a model was built at the University of Nevada, Reno using two large foam rubber blocks to simulate stick-slip ruptures with a strike-slip mechanism (Anooshehpoor and Brune, 2004). This model was used to generate more than 5000 strike-slip ruptures. This is equivalent to collecting nearly one million years of data from a fault with a 150-year return period such as the San Andreas Fault. This large dataset from the foam rubber provides the opportunity to perform robust statistical analyses on the distribution and variability of the "ground motions" recorded in the foam.

The main question we aim to answer with this study is whether these foam rubber ground motions are distributed according to a lognormal distribution. It is important to note that the foam rubber model and the crust of the earth are separate and distinct systems, and the findings of this statistical analysis do not necessarily translate to the earth system. However, the results from this study could help guide the continuing development of physical models. In addition to testing the distribution of

ground motions, we aim to compare the variability in the foam rubber ruptures with the variability of GMPE outputs. Thus, the focus of this paper is twofold: Firstly, to determine if a lognormal distribution is appropriate for describing peak ground motions in the foam rubber model, which can give insights into the behavior of repeated stick-slip ruptures, at least in this model. Secondly, to compare the variability of the model-generated peak ground motions with the variability given by the GMPE outputs in order to test the performance of the model.

Many people have been involved in the production of this work. My committee members are John Anderson, William Hammond and Edward Keppelmann, with Dr. Anderson serving as my advisor. The original experiment was run by Matthew Purvance, Rasool Anooshehpoor and James Brune. Matthew Purvance also performed the extraction of peak acceleration values and peak velocity values from the recorded seismograms. I performed the statistical analysis on the peak acceleration and velocity values.

Part II

Statistics of Ground Motions in a Foam Rubber Model of a Strike-Slip Fault

Kevin M. McBean, John G. Anderson, James N. Brune, Rasool Anooshehpoor

Abstract

The peak acceleration and velocity from 5058 ruptures of a foam rubber stick-slip model are not distributed according to a lognormal probability distribution function. PGA and PGV values are decomposed using the method of Anderson and Uchiyama (2011). The statistically significant deviations from the lognormal distribution occur near the peak of the distribution. In some cases, high-amplitude tails differ by a much greater ratio, but the statistical significance of this effect is low. This result is true of both raw data and data adjusted for site and magnitude. Event terms are also not lognormal, but can be modeled as a sum of three or four lognormal subdistributions, which possibly represent different preferred rupture initiation points rather than a uniform distribution of initiation points. The event term subdistributions with highest median values have small standard deviations, so if shapes of this nature were used in ground motion prediction equations (GMPEs) during a probabilistic seismic hazard analysis, the effect of the long tail of the lognormal distribution in controlling the hazard would be weakened considerably. Static stress drop was recorded for each event, and event terms for PGA and PGV are well correlated with static stress drop. Unlike NGAW2 GMPEs, residual variances for the foam model are dominated by variability in the source slip function, rather than the path and site effects. This difference in the variance budget results from the way in which the source and site residuals are defined in this study; the source uncertainty includes variation in the rupture size (magnitude) and location, along with deviations in distance and path. We do not know if these results apply to earthquakes but we do think tests of repeating stick-slip events in a physical system are useful to expand the set of credible hypotheses regarding possible behavior modes of earthquake faults.

Introduction

Modern probabilistic seismic hazard analysis (PSHA) requires a ground shaking model to predict ground motions at the site. These models are usually in the form of ground motion prediction equations (GMPEs), which are empirically calibrated from recordings of past earthquakes (e.g. Abrahamson et al., 2014). To be useful in PSHA, a GMPE must estimate both the amplitude and the uncertainty in the amplitude of a ground motion parameter as a function of magnitude and distance from the source (Strasser et al., 2009). Most GMPEs require additional predictor variables such as V_{S30}, depth of faulting, depth to bedrock, or fault type, to name a few.

If we let the ground motion parameter be Y, then GMPEs predict the median value of $G = \log Y$. Logarithmic transformations are commonly used in the development of GMPEs, however, the appropriateness of this method is not often rigorously tested. There are studies (Ambraseys et al., 2005 and Cauzzi and Faccioli, 2008) that tested the appropriateness of using the logarithmic transformation on recorded ground motions using the concept of pure error (Draper and Smith, 1981) and found that for several periods the logarithmic transformation was not justified. In both studies it was decided to use the logarithmic transformation anyway since its use was justified for neighboring periods. Douglas and Smit (2001) performed the same test on a different dataset and found that the logarithmic transformation was justified at all periods for that data. In determining the coefficients of the GMPEs, the residuals (differences in logarithms) from the prediction are assumed to be normally distributed (e.g. Bommer et al., 2004). Restrepo-Velez and Bommer (2003) found that the distribution of residuals seems to be consistent with the lognormal probability distribution except possibly in the tails. Yamada et al. (2009) found that, for near-source recordings of large earthquakes, peak ground accelerations are lognormally distributed and peak ground displacements are approximately uniformly distributed, even though they are lognormally distributed at a given magnitude. In detail, GMPE variation results from many processes: differing magnitudes and source properties, differing paths to each site, and, an inconsistent set of stations, that is, the set of stations recording one event typically has little to no overlap with the set recording a second event.

The use of a stick-slip physical model , which has a consistent set of stations and paths for each event, largely removes the effect of these contributions. Brune and others (Brune, 1973; Brune et al., 1989; Brune et al., 1993; Anooshehpoor and Brune, 1994) have modeled a stick-slip system with foam rubber blocks. They used two blocks to simulate strike-slip events as shown in Figure 1. The experiment is described in detail by Day et al. (2008).

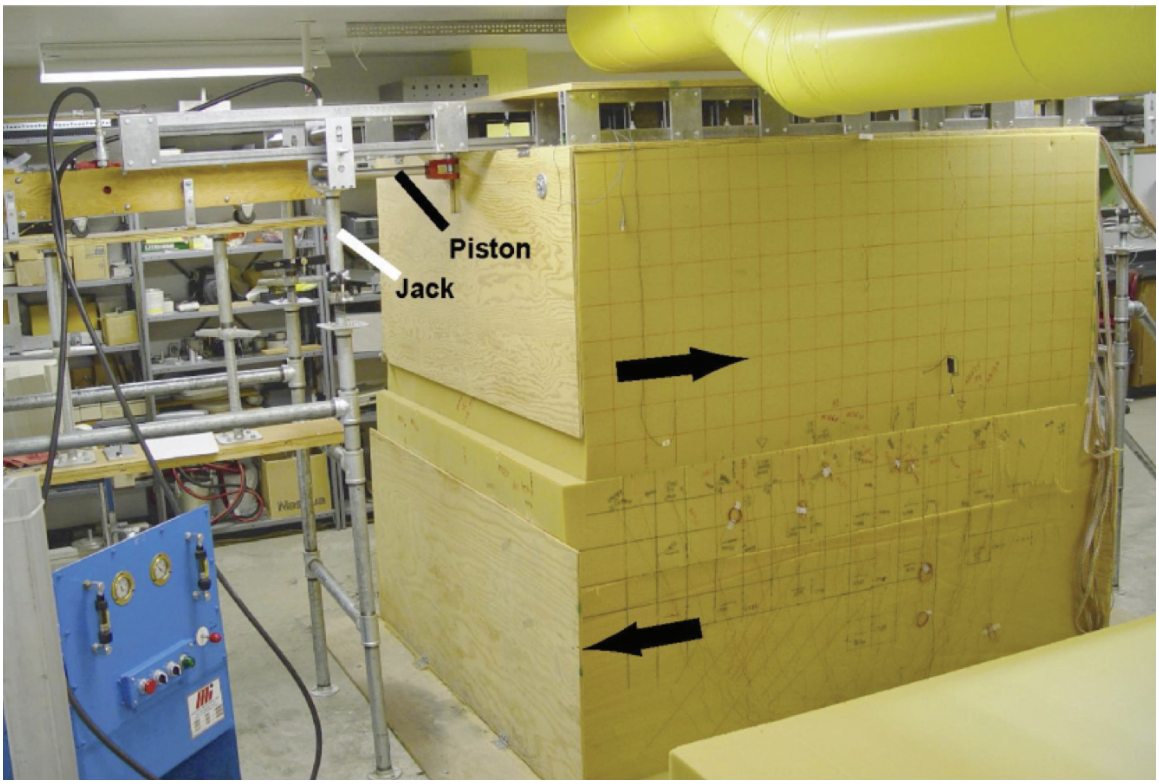

Figure 1: The foam model consists of two 2 m by 1.83 m by 0.95 m rubber foam blocks. The lower block is stationary, while the upper block is pushed by a hydraulic ram to produce small "ruptures" along the interface between the blocks. The model simulates a strike slip fault laid on its side; thus, the 28 accelerometers mounted on the closest side of the blocks are akin to seismometers placed on the ground surface near a strike slip fault. Image from Purvance et al., 2007.

Here we investigate the probability distribution functions (PDF) for the peak acceleration (PGA) and peak velocity (PGV) for 5058 foam rubber rupture events. Twenty-eight accelerometers located next to the geometrical equivalent of the fault trace recorded the events with 14 in a fault-parallel orientation and 14 in a fault-normal orientation. The sensors are mounted on styrofoam disks, which are mounted to the foam rubber. The foam rubber and styrofoam disks naturally filter some of the high frequency energy; however, no other filtering or processing to the recorded waveforms was performed. The details of the instrumentation are given in Brune and Anooshehpoor (1999).

Sample waveforms generated by a stick-slip rupture of the model are given in Figure 2. In these plots the sequence of initial arrivals coming at sequentially later times from station 15 to station 21 indicate that the rupture is propagating in that direction. The initial arrival increases in amplitude from station 15 to station 21, consistent with directivity from the rupture propagation. The increasing delay in the arrival of a second pulse moving backwards along the fault from station 21 to station 15 indicates that this second arrival has its origin near station 21; we interpret that as originating from the far end of the fault, perhaps as a breakout or stopping phase from when the rupture hits the end of the foam. Breakout and stopping phases are described by Savage (1965). While these breakout or stopping phases may not be present in the Earth, they are a feature of this model that generates accelerations from repeated ruptures in a physical system.

We compare the empirical distributions of PGA and PGV residuals with a lognormal distribution, focusing on the high tails of the distribution functions. The high tail is critical for evaluating hazard at very long return periods, e.g., for nuclear waste repositories as discussed by Stepp et al. (2001) and Abrahamson et al. (2002). For this experiment, the path is as uniform as possible, and the set of stations is the same for every event. Thus, the data we investigate reduces to a distribution of ground motions generated by variability of the source slip function.

Methods

The 5058 events took place over hundreds of runs, where on each run, 10 to 20 events occurred before the upper block had to be lifted and reset back to its original position. In Figure 3, which shows $ln(PGA)$ and $ln(PGV)$ for all events, there are two distinct populations. These populations are considered to be similar enough to be treated as one population in the analysis. We use the natural logarithm of PGA and PGV values, where a normal distribution of log space data is equivalent to a lognormal distribution of the peak values themselves.

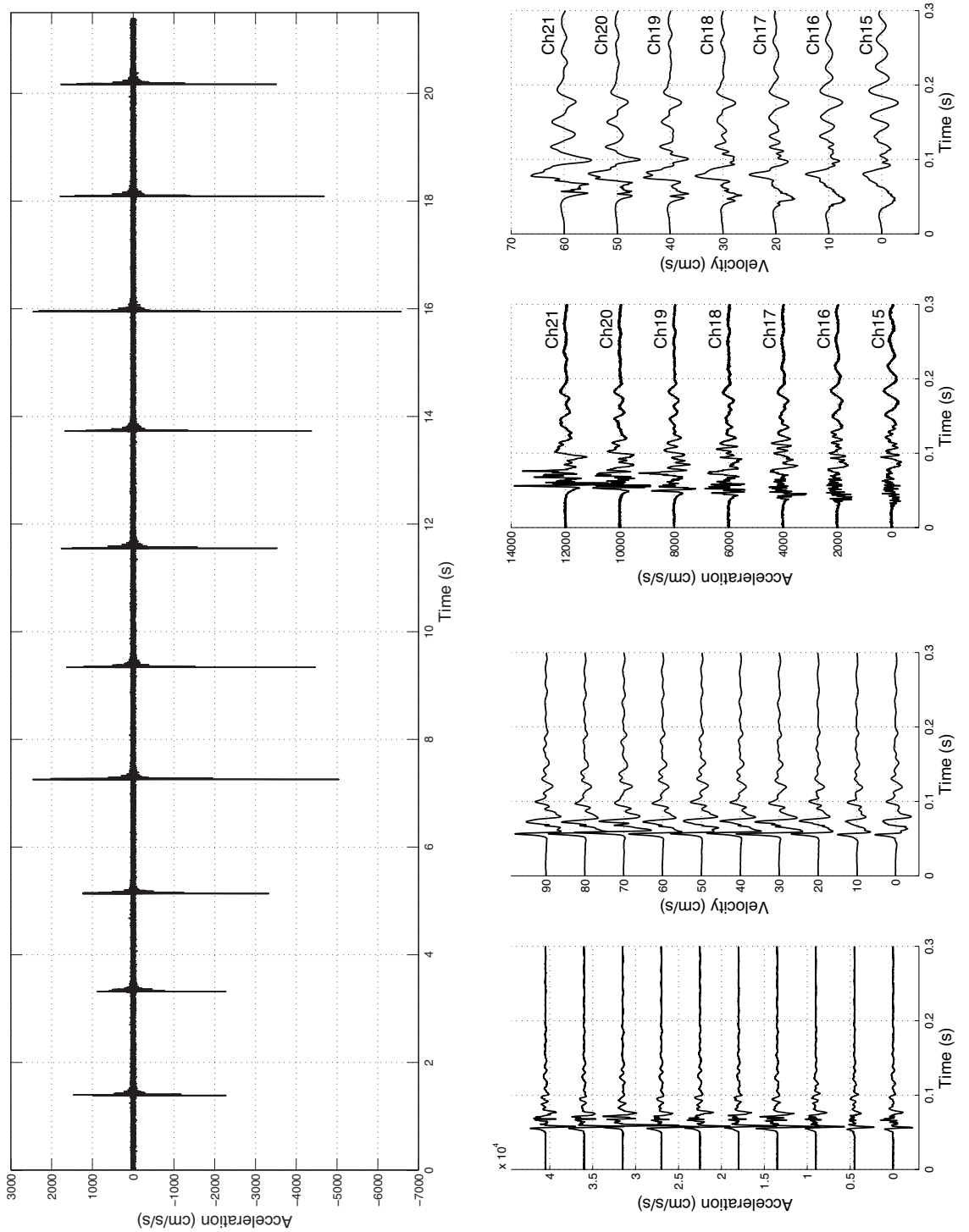

Figure 2: Waveforms recorded during one run of the experiment. The upper plot shows acceleration for one run of the experiment. The lower left plots present in detail the acceleration and velocity for each of the events in the upper plot. Each trace in the lower right plots corresponds to the time history of the event at 13.5 s as measured at one station.

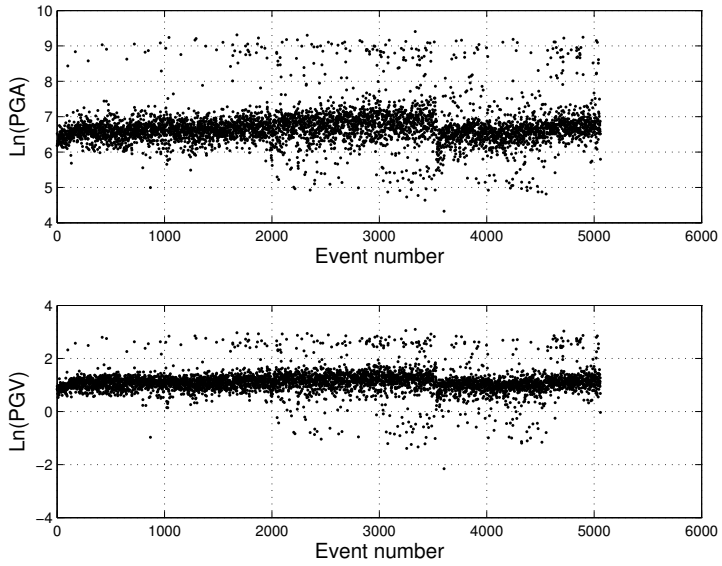

Figure 3: Peak ground accelerations and velocities at Station 1 as a function of event number.

Calculating Residuals

We use the method of Anderson and Uchiyama (2011) to model the observations of PGA and PGV by the sum of a regional excitation, event, and station term plus a residual. Since the data are in log space, subtracting mean values from the logarithm of the measurements results in residuals that are dimensionless.

The first residual, δ_{se}^{I}, is found by subtracting the regional excitation, which is the mean of all the 141,624 event/station values, $\bar{G}$, from all measurements. Thus,

$$G_{se} = \bar{G} + \delta_{se}^{I}, \tag{1}$$

where $G_{se} = \ln Y_{se}$, Y_{se} is the ground motion observation, and the subscripts s and e indicate the station number and event number, respectively. In a GMPE, $\bar{G}$ would be a function of magnitude and distance. In this experiment, most of the events rupture the entire foam interface. However, some of them do not, so in hindsight it would have been useful to develop some approach to determine the slip areas and mean slips independently. Since that was not done, the effects of variability of source size and sometimes dimension are all rolled into the event term that is determined subsequently. Also, since $\bar{G}$ is not a function of distance, the station terms that will be found subsequently are affected by location.

The station terms, S_s, are the average of the δ_{se}^{I} residuals across all events for station s; the standard deviation of the 28 station terms is σ_S. The second residual, δ_{se}^{II}, is calculated by subtracting the station term for a given station, S_s, from δ_{se}^{I}. Thus,

$$G_{se} = \bar{G} + S_s + \delta_{se}^{II} \tag{2}$$

Therefore, δ_{se}^{II} is the residual where the population mean and station mean have been removed.

The event terms, E_e, are the average of the δ_{se}^{II} residuals across all stations for event e; the standard deviation of the event terms is σ_E. Sensitivity tests found that the station and event terms are nearly independent of the order in which they are determined. The third residual, δ_{se}^{III}, is found by subtracting the event term for a given event from the second residual. Therefore,

$$G_{se} = \bar{G} + S_s + E_e + \delta_{se}^{III}. \tag{3}$$

Thus, δ_{se}^{III} is what remains after removing the population, station, and event means. If the distributions of S_s, E_e, and δ_{se}^{III} are approximately normal, and assuming the residuals are uncorrelated, we find:

$$\left(\sigma^{I}\right)^2 = \sigma_S^2 + \left(\sigma^{II}\right)^2 = \sigma_S^2 + \sigma_E^2 + \left(\sigma^{III}\right)^2, \tag{4}$$

where σ^{I}, σ^{II}, and σ^{III} are the standard deviations of δ_{se}^{I}, δ_{se}^{II}, and δ_{se}^{III}, respectively. As noted earlier, event and site terms, E_e and S_s, are not equivalent to those in a GMPE or in Anderson and Uchiyama (2011). Therefore, values of σ^{I}, σ_S, and σ_E are not equivalent to σ_T, ϕ, and τ in the typical GMPE notation. In the GMPE notation, σ_T is the total uncertainty, ϕ is the within-event standard deviation, and τ is the between-event standard deviation. The standard deviation of the residuals after removing event terms, σ^{III}, is most comparable to the GMPE within-event, single-site sigma (ϕ_{SS} in the Al Atik et al., 2010 notation). The approach in equations 1 through 4 is actually closer to the averaging-based factorization (ABF) method of Wang and Jordan (2014).

Checking the Fit of the Data to a Log-Normal Distribution

We use the non-parametric Kolmogorov-Smirnov (K-S) statistical test (Massey, 1951) to check the fit of the data to a lognormal distribution. The complementary cumulative distribution function (CCDF), where $CCDF = 1 - CDF$, and CDF is the cumulative distribution function, plotted on a semi-log axis emphasizes the shape of the upper tail of the distribution. The difference between the

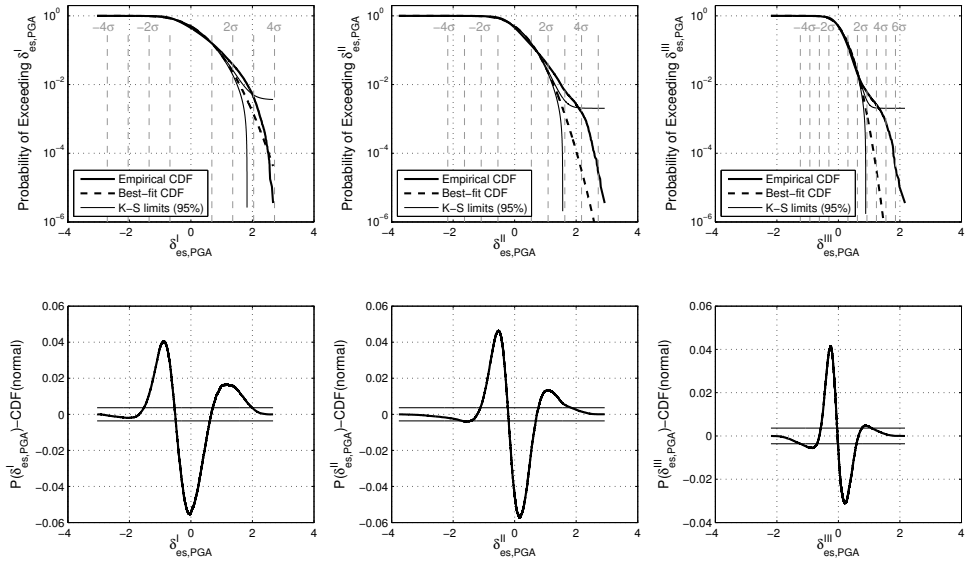

Figure 4: CCDF of δ_{se} for PGA. The heavy black lines are the empirical CDFs; the dashed line in the upper plots is a "best-fit" normal CDF with the same mean and variance as the data. The light black lines are the Kolmogorov-Smirnov limits at the 95% confidence level. The lower plots show the difference between the empirical and best-fit CDFs with the K-S limits indicated by the light lines. Grey dashed lines indicate the number of standard deviations from the mean.

Table 1: Model standard deviations

	PGA	PGV
σ^I	0.680	0.564
σ^{II}	0.543	0.468
σ^{III}	0.309	0.236
σ_E	0.447	0.404
σ_S	0.415	0.319

empirical CCDF, derived from one of the δ residuals or E_e and the best-fit CCDF (a CCDF with the mean and standard deviation equal to the empirical CCDF) is compared with the 95% confidence bounds obtained from the K-S test.

Results

PGA Residuals

Figure 4 shows plots of the CCDF of the PGA residuals δ^I_{se}, δ^{II}_{se}, and δ^{III}_{se}. By construction, the mean of each distribution is zero. The corresponding standard deviations of the residuals, σ^I, σ^{II}, and σ^{III}, for PGA and PGV are given in Table 1. The standard deviations of the station and

Table 2: NGAW2 Standard deviations

	PGA				PGV			
	ASK14	BSSA14	CB14	CY14	ASK14	BSSA14	CB14	CY14
σ_T	0.617	0.605	0.578	0.553	0.636	0.652	0.576	-
ϕ	0.501	0.495	0.485	-	0.510	0.552	0.494	-
τ	0.360	0.348	0.314	0.260	0.380	0.346	0.297	-

event terms, σ_S and σ_E, are determined from the values of S_S and E_E, so Equation 4 is only approximately satisfied. It should be noted that $\sigma^I > \sigma^{II} > \sigma^{III}$. The lower set of plots in Figure 4 shows the difference between the empirical CDF and the normal CDF with mean and standard deviation equal to the mean and standard deviation of the data. Table 2 gives σ values for the Next Generation Attenuation-West2 (NGAW2) GMPEs (Abrahamson et al., 2014 (ASK14); Boore et al,. 2014 (BSSA14); Campbell and Bozorgnia, 2014 (CB14); and Chiou and Youngs, 2014 (CY14)). Table 2 is included for reference, but as noted above, σ^I, σ^{II}, σ^{III}, σ_S, and σ_E are not strictly equivalent to the NGAW2 σ values.

The distributions of all three types of PGA residuals are outside the 95% confidence limits for some portion of the distribution, including values near the mean. We can thus reject the hypothesis that the PGA residuals are lognormally distributed, even after removing the variability captured in the station and event terms.

The high tails of the empirical CDFs for both δ_{se}^{II} and δ_{se}^{III} have a higher probability of exceedance than the best-fit CDF, but they are within the 95% limits. At slightly lower values of the residuals, there are many more data points, yet the probability of exceedance still remains higher (by $\sim 10^1$) for the empirical CDFs. Additionally, the empirical distributions fall outside the K-S limits between approximately 2σ and 4σ. The highest PGA values in the foam model occur more frequently than what would be predicted by a log-normal distribution.

PGV Residuals

The results for PGV are similar to the results for PGA. Figure 5 shows the CDFs for the PGV residuals and Table 1 gives the PGV standard deviations. As with PGA, the PGV empirical CDFs do not fit a lognormal distribution at the 95% confidence level. For PGV, as with PGA, $\sigma^I > \sigma^{II} > \sigma^{III}$ and the δ_{se}^{III} distribution is around an order of magnitude higher than the best-fit CDF in the mid-high tail. Thus, as with PGA, we can reject the hypothesis that the PGV residuals in this system are lognormally distributed after removing the station and event terms.

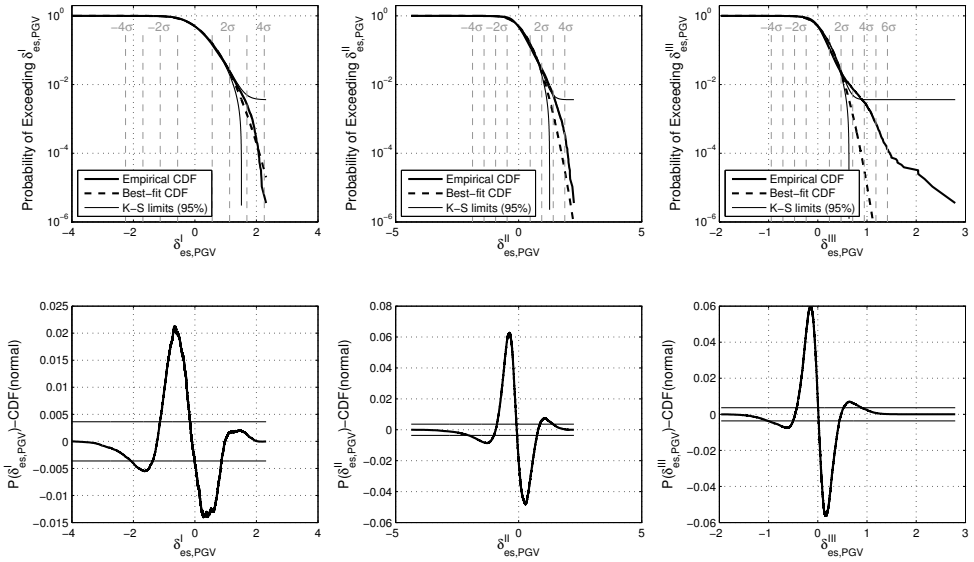

Figure 5: CCDF of δ_{se} for PGV.

Event and Station Terms

The distributions of event terms for PGA and PGV are shown in Figure 6; they also are not consistent with a lognormal distribution. The standard deviations of the event terms, σ_E, are given in Table 1. Note that, as expected, σ_E is larger than σ^{III} or σ_S. Thus, the main source of variability in this experiment is the variability among the ruptures.

It is interesting to note that that the CCDF in the PGA and PGV event terms in Figure 6 decrease almost vertically for probabilities below $\sim 10^{-3}$, suggesting that there may be a natural maximum event size at around 3σ. While these bounds may not be significant in the statistical sense because the distribution of the data is within the K-S limits, it makes physical sense that there is a bound on the event size imposed by the strength of the fault subjected to the experimental boundary conditions.

Figure 7 compares PGA and PGV event terms and finds that they are very closely correlated (correlation coefficient of 0.96). Considering that PGA and PGV are controlled by different frequencies of wave motions, the simplest way to explain this correlation is if the foamquake sources obey a scaling law for the seismic spectrum analogous to earthquakes (e.g. Aki, 1967). The amplitude of the seismic spectrum has first order dependencies on the fault dimension and the source-station distance. Both of these are assumed to be represented in the data. We assume that some small

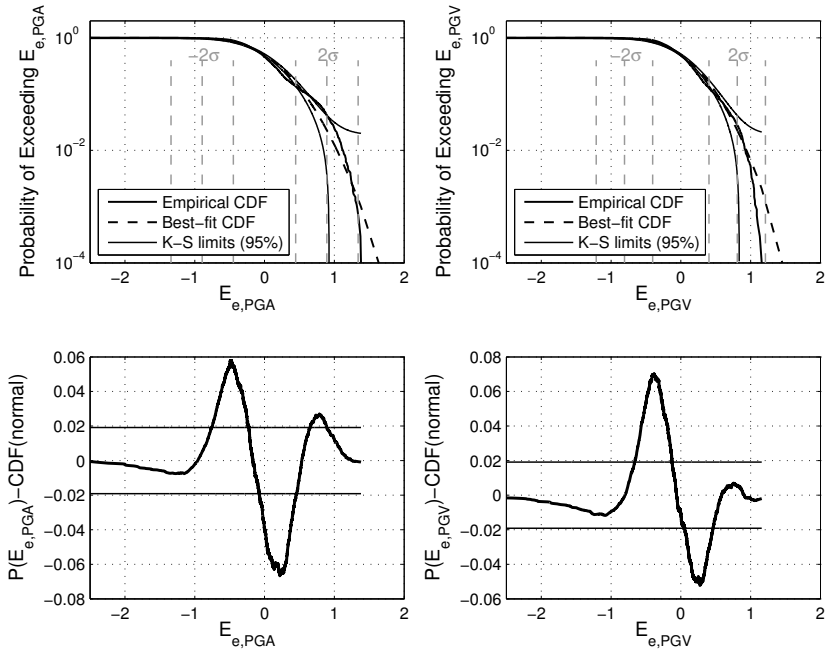

Figure 6: CCDF of event terms for PGA and PGV. The distributions of event terms fall well outside the 95% confidence intervals for both PGA and PGV.

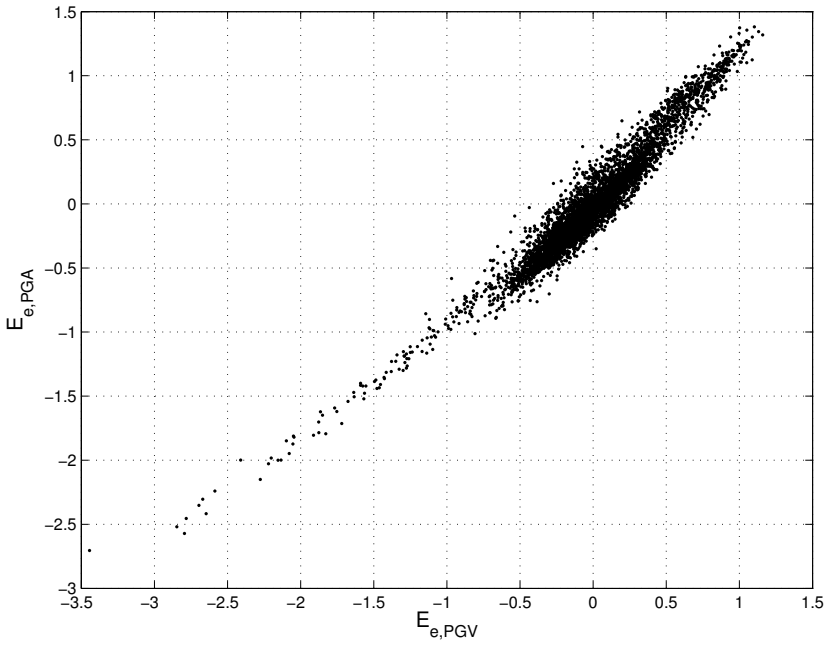

Figure 7: PGA and PGV event terms are very well correlated. Note a change in slope near (0,0).

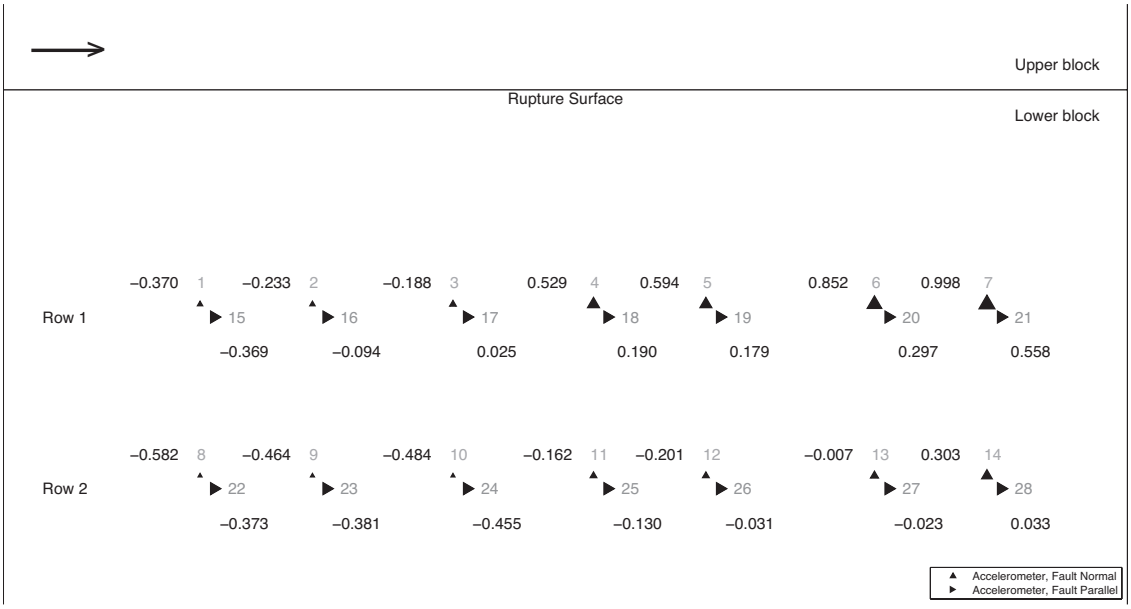

Figure 8: The station layout and the station terms for PGA. The grey number is the station number; the black number is the station term for that station. The triangles indicate the location of the sensors and their size correlates with the station term value. The outline of the foam rubber block and station locations are drawn to scale. The block width is 2 m.

fraction of the foamquakes rupture only a small patch of the total interface and that those patches can be at different distances from the sensors. We further assume some foamquakes have a larger mean slip than others. Thus, E_e incorporates both magnitude and distance adjustments and fills in for both of these effects in Equation 3.

The station terms for PGA and PGV and their relative locations are presented in Figures 8 and 9. The station terms are generally higher on row 1 for both PGA and PGV, as expected. At the same distance to the fault, the station terms tend to increase toward the right-hand side of the model. This is caused by a tendency for the rupture to initiate on the left of the model, where the driving piston is located, and propagate to the right. Thus, the higher numbered stations within a single row are, more often than not, in a direction of forward directivity. Along row 1, the station term on the fault-normal sensors farthest from the piston tends to be larger than on the corresponding fault-parallel sensor, consistent with expectations of a forward-directivity pulse to have a strong fault-normal component (Somerville, 2003). Along row 2 for PGA and PGV, the fault-parallel sensors tend to have a higher station term than the corresponding fault-normal sensor. This suggests that for these stations, because of their geometry relative to the fault, the dominant process is the radiation pattern rather than directivity.

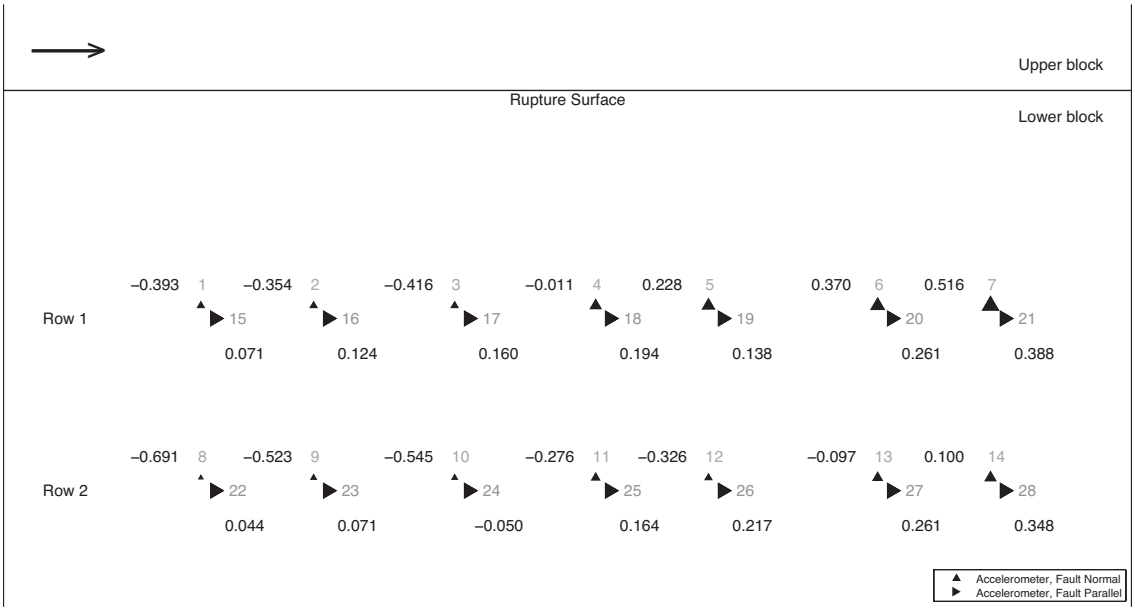

Figure 9: Station layout and station terms for PGV.

Single Station Distributions

The PGA and PGV distribution functions of δ_{se}^{III} for each station are shown in Figures 10 and 11. For both PGA and PGV, left-hand stations in row 1 have high tail residual bumps. In general, stations closer to the right-hand side of the model have lower probabilities of exceeding a given δ_{se}^{III} residual value. The δ_{se}^{III} residuals do not contain average effects captured by S_s and E_e; thus, differences in δ_{se}^{III} distributions can only be caused by differences from average effects. The higher probabilities of exceedance of δ_{se}^{III} residuals for left-hand stations suggested to Purvance et al. (2007) that distinct rupture modes contributed to these probability distributions.

Inversion

After finding that a simple lognormal distribution does not fit the event terms or the residuals in Equations 2 or 3, we modeled the PGA and PGV event term distributions using a sum of multiple lognormal CDFs with a combination of inversion and trial-and-error. The inversion uses the form

$$Gm = d, \tag{5}$$

where d is an $n \times 1$ vector that contains a concatenation of the empirical CDF and its CCDF. Using the CCDF in addition to the CDF gives more weight to the high tail than using the CDF alone. G is

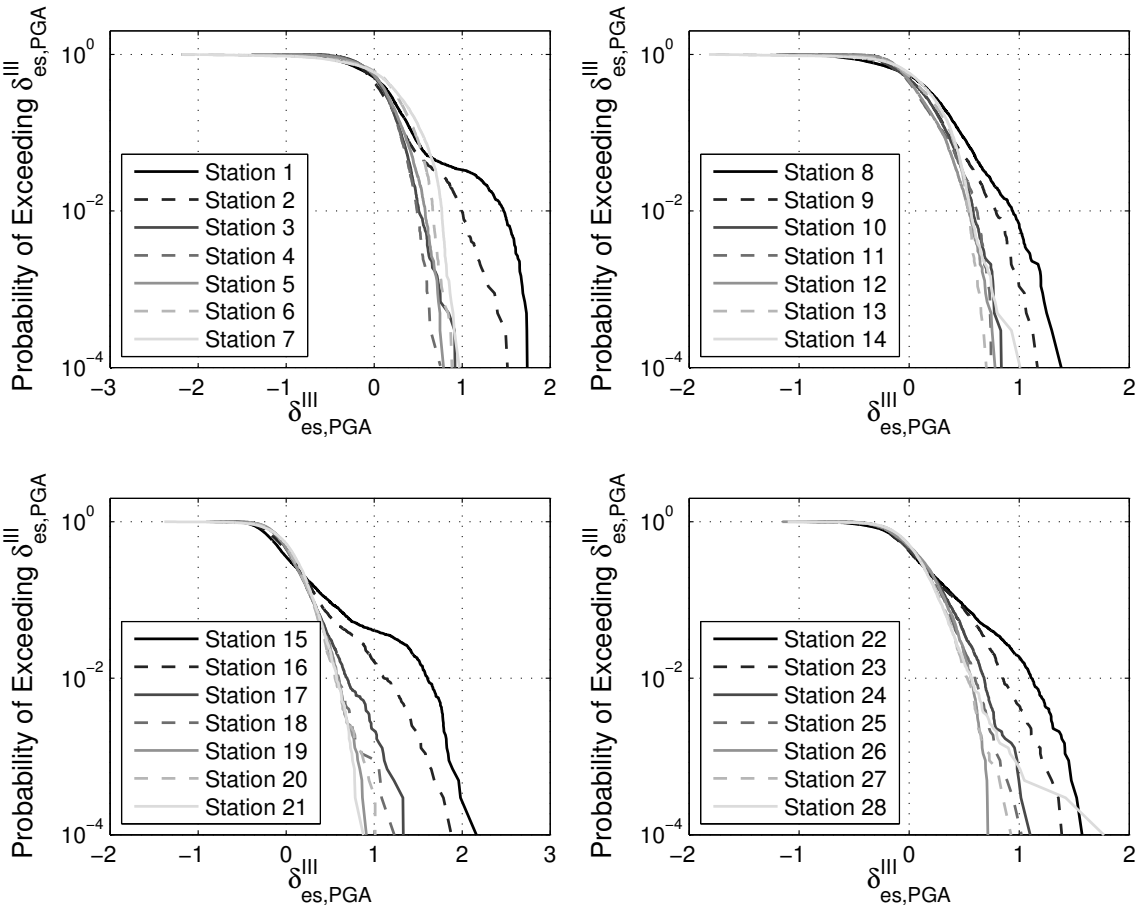

Figure 10: Single station distributions for $\delta^{III}_{se,PGA}$.

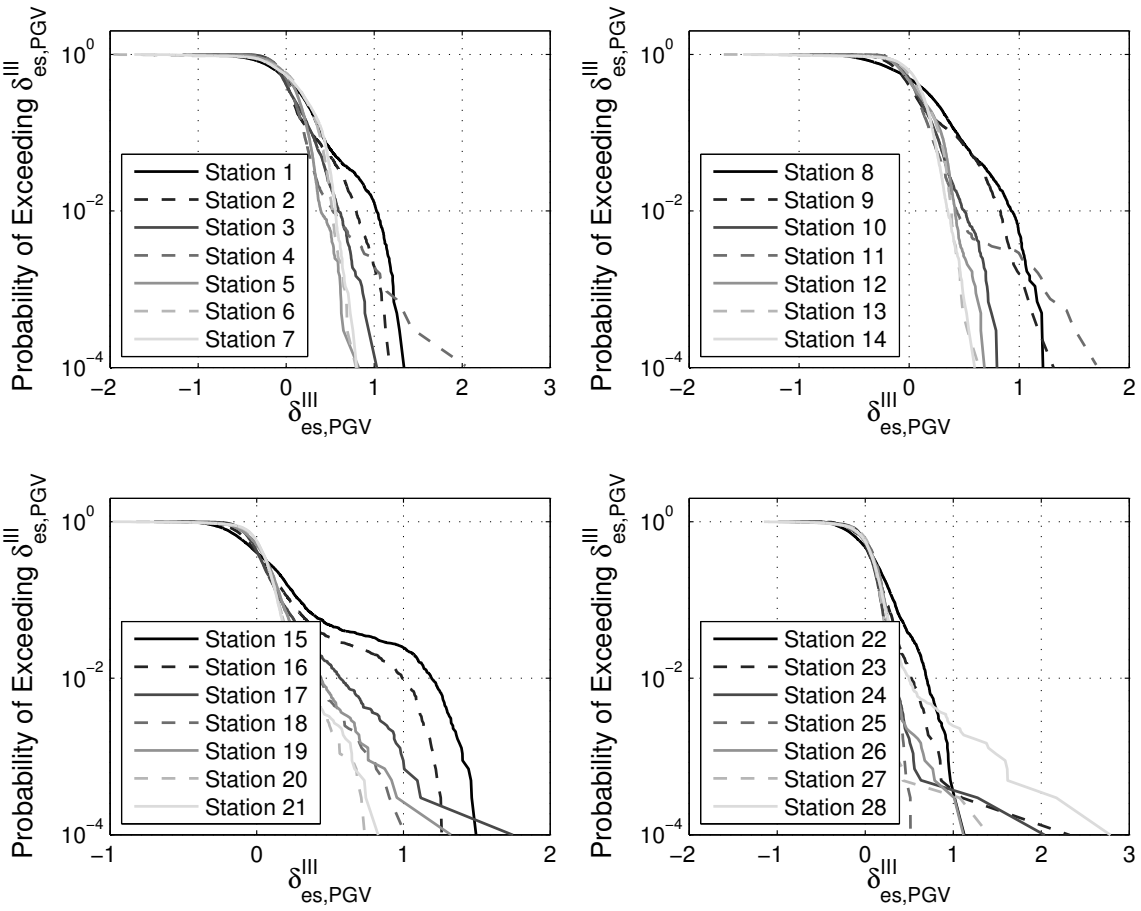

Figure 11: Single station distributions for $\delta^{III}_{se,PGV}$.

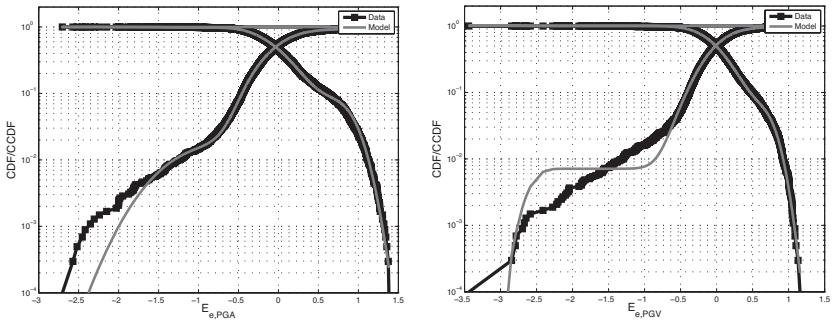

Figure 12: Event term inversion results for PGA and PGV. CDF and CCDF are both represented.

Table 3: Event term model parameters

	PGA				PGV		
Model CDF	1	2	3	4	1	2	3
μ	-1.36	-0.34	-0.025	0.94	-2.60	-0.03	0.80
σ	0.40	0.16	0.30	0.16	0.15	0.30	0.13
Weight	0.018	0.090	0.811	0.082	0.007	0.947	0.054

an $n \times p$ matrix containing column vectors of the model CDFs to be tested. The vector m is an $p \times 1$ element that contains the weights of each model CDF, as determined by the inversion algorithm. In an acceptable model, the sum of the elements of m is 1.0. The mean (μ_i) and standard deviation (σ_i) of the model CDFs were chosen in an iterative trial-and-error process, with the goal of finding the minimum number of model distributions necessary to obtain a reasonable fit to the data. The model was considered to be a good fit if the weights (m_i) were all positive, σ^2 (the normalized sum of the square of the residuals between the data and the model) had a low value, and a visual inspection revealed a close alignment of the data and the weighted sum of the model CDFs. Sensitivity tests of the inversion algorithm indicate that it can resolve a separation between two model CDF means as small as 0.01. The inversion accurately determines model weights to less than 0.0001.

Modeling the event terms with a sum of three or four distributions produced acceptable results. Adding more distributions did not improve the fit significantly. Using a larger number of distributions reduced σ^2 , however the inversion uses negative weights to produce such a fit.

Figure 12 shows the fit of the models to the PGA and PGV event term distributions. Table 3gives the parameters of the model CDFs for PGA and PGV. Both distributions are reasonably well approximated as the sum of lognormal subdistributions, especially for larger event term values. The ability to model the event terms in this way suggests that there is a finite number of preferred rupture modes in the model. We speculate that preferred rupture modes could be more strongly

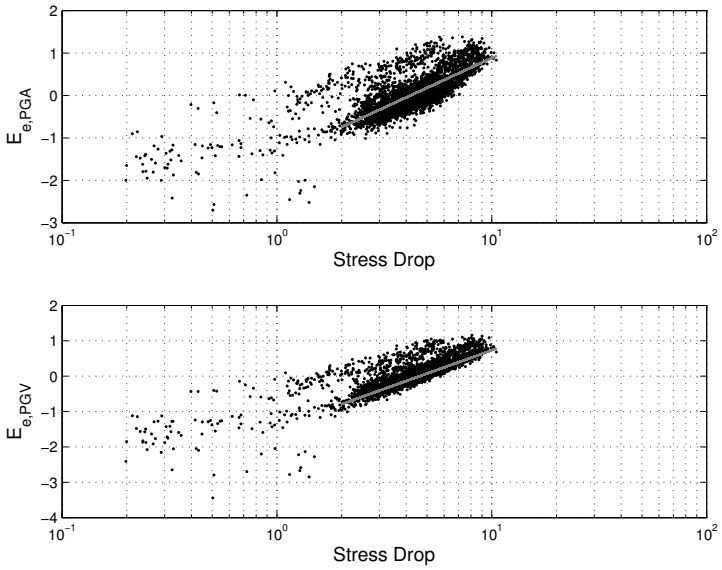

Figure 13: Correlation of PGA and PGV event terms with stress drop.

Table 4: Correlation of stress drop with event terms

	a	b	corr. coeff.
$E_{e,PGA}$	1.01 ± 0.15	-1.45	0.76
$E_{e,PGV}$	0.95 ± 0.08	-1.44	0.82

expressed in the Earth than in the foam model, because the Earth is far more heterogeneous. If that is true, the distribution of event terms from a single fault in the Earth might be narrow, like the distributions of individual components of the CDF models in Figure 12.

Stress Drop

Absolute stress was recorded before and after each rupture event. From these stress values we calculated the static stress drop in the model during a rupture. The correlation of stress drop with both PGA and PGV event terms is given in Figure 13. The event terms are well correlated with stress drop for stress drop values greater than 2. The best-fit takes the form:

$$E_e = a[ln(\Delta\tau)] + b, \tag{6}$$

where $\Delta\tau$ is the stress drop. The values of a, b, and the correlation coefficients are given in Table 4. Within error, for both PGA and PGV, the event terms are directly proportional to stress drop.

Event terms can thus be predicted from stress drop with an uncertainty of 1.06 for $E_{e,PGA}$ and 1.11 for $E_{e,PGV}$.

Discussion and Conclusions

The contributions to the variability of peak acceleration and peak velocity measurements in the foam rubber model and in the NGAW2 GMPEs were tabulated in Tables 1 and 2, respectively. In the foam model, the event terms (E_e) contribute most to the total variability, but, unlike in GMPEs, these terms also include effects of distance and magnitude. Thus, the values of the variability in the event terms, σ_E, are considerably higher than the values of τ given by the NGAW2 GMPEs. In GMPEs, the station residuals include the variability introduced by the ergodic assumption (Anderson and Brune, 1999), while in the foam, the site conditions are more uniform. This explains why the variability due to station terms, σ_S in Table 1, is smaller than ϕ in Table 2. The standard deviation σ^{III} is most comparable to the event-corrected, single-station standard deviation, ϕ_{SS}, as discussed by Rodriguez-Marek et al. (2011). Our estimates of σ^{III} are 0.31 for PGA and 0.24 for PGV and are thus smaller than the range of ϕ_{SS} found by Rodriguez-Marek et al (2011), which are from 0.39-0.51 over a range of response spectral periods.

We reject the hypothesis that peak accelerations and peak velocities in the foam rubber model are lognormally distributed. The most significant deviations are near the median value of the distribution. If the type of deviation seen in Figures 4 and 5 were true of ground motion parameters in the Earth, these deviations would have some impact on hazard estimates but the effect would be small. For instance, consider a target hazard of 2% in 50 years, which corresponds to an occurrence rate of 1/2475 per year. Consider also a site near an active fault such as the San Andreas fault that has an average recurrence interval of 1/150 years. The target hazard level is at a rate of 0.06 times the recurrence interval on the fault. Considering Figures 4 and 5, the hazard estimate for this case is impacted by the horizontal distance between the lognormal assumption and the empirical CCDF at an exceedance level of 0.06. For $\delta^{I}_{es,PGA}$, where there has been no adjustment for site or magnitude, the difference is $e^{0.14}$, which would be an increase in the hazard of 1.15. For $\delta^{III}_{es,PGA}$, where site and magnitude have been adjusted for, the difference is $-e^{0.04}$, which would decrease the hazard by 1.04. For a critical facility where a longer return period must be considered, it is necessary to use smaller exceedance values on the CCDF where the difference between the curves, and thus the effect on the hazard, is more significant.

In the foam, the distributions of δ_{es}^{II} and δ_{es}^{III} have a heavier tail than the lognormal distribution; although, the statistical significance of this feature is smaller than the 95% confidence criterion we prefer. This heavy tail can be approximated by considering the complete PDF to be a sum of several distributions, as suggested by Purvance et al. (2007), which is representative of different rupture modes on the fault. If these heavy tails also occur in Earth ground motions, the beneficial element for PSHA is that they have a very small standard deviation.

A particularly interesting result from this analysis is the correlation of PGA and PGV event terms with stress drop. The correlation suggests that, at least in the foam model, peak motions are directly correlative to stress drop. Brune (1970) states that, in the near-field, particle velocity is proportional to effective stress and the ratio of shear velocity to shear modulus. So, based on the physics of stick-slip, we would expect velocity and acceleration to be proportional to stress drop in the near-field. However, since in the foam the peak values are recorded at near-field distances, far-field statistics might have different properties.

These results are only relevant if we can accept that a foam block model is representative of the physical earth system. This has, of course, been a subject of much discussion. Arguments in favor of their relevance have been presented in several studies (e.g. Hartzell and Archuleta, 1979 and Brune and Anooshehpoor, 1999). The foam has a Poisson's ratio of about 0.25, like rock at seismogenic depths, so the distribution of P- and S-wave energy in stick-slip events should be comparable. Also, the rupture velocity in foam, about 0.7β, is similar to that of the earth. The strains in the foam model are on the order of 10^{-2}, which is higher than in the earth (on the order of 10^{-4}); however, Hartzell and Archuleta (1979) found that, even with the larger strains, the foam behaves linearly.

The coefficient of friction between the blocks is greater than values for rock under seismogenic conditions found in laboratory experiments (˜0.85). However, the initiation of slip in the foam model is not fully dependent on the coefficient of friction. It also depends on the distribution of strain in the bulk volume in the direction of dynamic rupture propagation as a result of a dynamic reduction of normal stress or even partial separation of the block. This mechanism is perhaps plausible in light of the low heat generation (see Anooshehpoor and Brune, 1994) on the fault, some theoretical concepts such as Schallamach waves, and numerical studies (Day et al., 2008).

Whether or not it is appropriate to extrapolate these results to earthquakes will remain an open question. In either case, these findings result from an analysis of ground motions from a large number of repeated ruptures in a real, physical stick-slip system. If they do extrapolate, the deviation from the lognormal CDF near the median would probably have a small impact on the outcome of a PSHA.

The particularly important features are the very narrow subdistributions at the high amplitudes, giving a very rapid decrease in exceedance probabilities at the highest amplitudes observed in the system.

Data Sources

The experiment reported here was executed by Matthew Purvance, James Brune, and Rasool Anooshehpoor. Extraction of the peak acceleration and peak velocity values from the original seismograms was performed by Matt Purvance.

Acknowledgments

This study was motivated by Edward Keppelmann's probability theory class at the University of Nevada, Reno; we wish to thank him for his support. We would also like to thank Benjamin Edwards and an anonymous reviewer for their helpful suggestions to the original manuscript and Matthew Purvance for providing the data used in this paper. This project has received support of the Southern California Earthquake Center and is SCEC Proposal Number 07080.

References

Abrahamson, N., P. Birkhauser, M. Koller, D. Mayer-Rosa, P. Smit, C. Sprecher, S. Tinic, and R. Graf (2002). PEGASOSA comprehensive probabilistic seismic hazard assessment for nuclear power plants in Switzerland, in Proceedings of the 12th European Conference on Earthquake Engineering, London, Paper No. 633.

Abrahamson, N. A. (2006). Seismic hazard assessment: problems with current practice and future developments. In first European conference on earthquake engineering and seismology, Geneva, Switzerland, pp. 3-8.

Abrahamson, N. A., W. J. Silva, and R. Kamai (2014). Summary of the ASK14 ground motion relation for active crustal regions, Earthq. Spectra 30, no. 3, 1025–1055, doi: 10.1193/070913EQS198M.

Aki, K. (1967). Scaling law of seismic spectrum, J. Geophys. Res. 72, 1217– 1231, doi: 10.1029/JZ072i004p01217.

Al Atik, L., N. Abrahamson, J. J. Bommer, F. Scherbaum, F. Cotton, and N. Kuehn (2010).

The variability of ground-motion prediction models and its components, Seismol. Res. Lett. 81, 794–801, doi: 10.1785/ gssrl.81.5.794.

Ambraseys, N. N., J. Douglas, S. K. Sarma, and P. M. Smit (2005). Equations for the estimation of strong ground motions from shallow crustal earthquakes using data from Europe and the Middle East: Horizontal peak ground acceleration and spectral acceleration, Bull. Earthq. Eng. 3, no. 1, 1–53, doi: 10.1007/s10518-005-0183-0.

Anderson, J. G., and J. N. Brune (1999). Probabilistic seismic hazard assessment without the ergodic assumption, Seismol. Res. Lett. 70, no. 1, 19–28.

Anderson, J. G., and Y. Uchiyama (2011). A methodology to improve ground-motion prediction equations by including path corrections, Bull. Seismol. Soc. Am. 101, 1822–1846.

Anooshehpoor, A., and J. N. Brune (1994). Frictional heat generation and seismic radiation in a foam rubber model of earthquakes, Pure Appl. Geophys. 142, 735–747.

Anooshehpoor, A. and J. N. Brune. (2004) "Study of Rupture Directivity in a Foam Rubber Physical Model," PEER Lifeline Task 1D01 Report, Pacific Earthquake Engineering Research Center.

Bommer, J. J., N. A. Abrahamson, F. O. Strasser, A. Pecker, P.-Y. Bard, H. Bungum, F. Cotton, D. Fäh, F. Sabetta, F. Scherbaum, and J. Studer (2004). The challenge of defining upper bounds on earthquake ground motions, Seismol. Res. Lett. 75, no. 1, 82–95.

Boore, D. M., J. P. Stewart, E. Seyhan, and G. M. Atkinson (2014). NGA-West 2 equations for predicting PGA, PGV, and 5% damped PSA for shallow crustal earthquakes, Earthq. Spectra 30, no. 3, 1057–1085, doi: 10.1193/070113EQS184M.

Brune, J. N. (1970), Tectonic stress and spectra of seismic shear waves from earthquakes, J. Geophys. Res. 75, 4997-5009.

Brune, J. N. (1973). Earthquake modeling by stick-slip along pre-cut surfaces in stressed foam rubber, Bull. Seismol. Soc. Am. 63, 2105–2119.

Brune, J. N., and A. Anooshehpoor (1999). Dynamic geometrical effects on strong ground motion in a normal fault model, J. Geophys. Res. 104, 809–815.

Brune, J. N., S. Brown, and P. A. Johnson (1993). Rupture mechanism and interface separation in foam rubber models of earthquakes: A possible solution to the heat flow paradox and the paradox of large overthrusts, Tectonophysics 219, 59–67.

Brune, J. N., P. A. Johnson, and C. Slater (1989). Constitutive relations for foam rubber stick-slip, Seismol. Res. Lett. 60, 26.

Campbell, K. W., and Y. Bozorgnia (2014). NGA-West 2 ground motion model for the average horizontal components of PGA, PGV, and 5% damped linear acceleration response spectra, Earthq. Spectra 30, no. 3, 1087–1115, doi: 10.1193/062913EQS175M.

Cauzzi, C., and E. Faccioli (2008). Broadband (0.05 to 20 s) prediction of displacement response spectra based on worldwide digital records, J. Seismol. 12, no. 4, 453–475, doi: 10.1007/s10950-008-9098-y.

Chiou, B. S.-J., and R. R. Youngs (2014). Update of the Chiou and Youngs NGA model for the average horizontal component of peak ground motion and response spectra, Earthq. Spectra 30, no. 3, 1117–1153, doi: 10.1193/072813EQS219M.

Day, S. M., S. H. Gonzalez, R. Anooshehpoor, and J. N. Brune (2008). Scale-model and numerical simulations of near-fault seismic directivity, Bull. Seismol. Soc. Am. 98, 1186–1206.

Douglas, J., and P. M. Smit (2001). How accurate can strong ground motion attenuation relations be? Bull. Seismol. Soc. Am. 91, no. 6, 1917–1923, doi: 10.1785/0120000278.

Draper, N. R., and H. Smith (1981). Applied Regression Analysis, Second Ed., Wiley, New York, New York.

Hartzell, S. H., and R. J. Archuleta (1979). Rupture propagation and focusing of energy in a foam rubber model of a stick slip earthquake, J. Geophys. Res. 84, 3623–3636.

Massey, F. J. (1951). The Kolmogorov–Smirnov test for goodness of fit, J. Am. Stat. Assoc. 253, 68–78.

Petersen, M. D., M. Moschetti, P. Powers, C. Mueller, K. Haller, A. Frankel, Y. Zeng, S. Rezaeian, S. Harmsen, O. Boyd, N. Field, R Chen, K. Rukstales, N. Luco, R. Wheeler, R. Williams, and A. Olsen (2014). Documentation for the 2014 update of the United States national seismic hazard maps: U.S. Geological Survey Open-File Report 2014–1091, 243 p., http://dx.doi.org/10.3133/ofr20141091.

Purvance, M., J. G. Anderson, R. Anooshehpoor, and J. N. Brune (2007). Statistics of ground motions in a physical system, SCEC Annual Report 2007.

Restrepo-Velez, L. F., and J. J. Bommer (2003). An exploration of the nature of the scatter in ground motion prediction equations and the implications for seismic hazard assessment, J. Earthq. Eng. 7, no. 1,171–199.

Rodriguez-Marek, A., G. A. Montalva, F. Cotton, and F. Bonilla (2011). Analysis of single-station standard deviation using the KiK-net data, Bull. Seismol. Soc. Am. 101, 1242–1258.

Romeo, R., and A. Prestininzi (2000). Probabilistic versus deterministic seismic hazard analysis: an integrated approach for siting problems, Soil Dynamics and Earthquake Engineering, 20, 75-84.

Savage, J. C. (1965). The stopping phase on seismograms, Bull. Seismol. Soc. Am. 55, 47–58.

Somerville, P. G. (2003). Magnitude scaling of the near fault rupture directivity pulse, Phys. Earth Planet. In. 137, 201–212.

Stepp, J. C., I. Wong, J. Whitney, R. Quittemeyer, N. Abrahamson, G. Toro, R. Youngs, K. Coppersmith, J. Savy, T. Sullivan, and Yucca Mountain PSHA project members (2001). Probabilistic seismic hazard analyses for ground motions and fault displacements at Yucca Mountain, Nevada, Earthq. Spectra 17, no. 1, 113–151.

Strasser, F. O., N. A. Abrahamson, and J. J. Bommer (2009). Sigma: Issues, insights and challenges, Seismol. Res. Lett. 80, no. 1, 40–54.

Wang, F., and T. H. Jordan (2014). Comparison of probabilistic seismic-hazard models using averaging-based factorization, Bull. Seismol. Soc. Am. 104, 1230–1257.

Yamada, M., A. H. Olsen, and T. H. Heaton (2009). Statistical features of short-period and long-period near-source ground motions, Bull. Seismol. Soc. Am. 99, no. 6, 3264–3274, doi: 10.1785/0120090067.

Part III

Conclusions and Recommendations

The aim of this study was to determine if the peak ground motions generated by a physical stick-slip model are lognormally distributed. A second component of the study was to compare the uncertainty in the peak ground motions with the uncertainty given by the NGAW2 GMPEs. We will first discuss the results of the uncertainty analysis.

After removing the uncertainty from the event terms, σ_E, which reflects the variability in the magnitude of the ruptures, and also after removing the uncertainty from the station terms, σ_S, which is introduced by variability at the accelerometers, we are left with σ^{III}. This last term, σ^{III}, includes all remaining sources of uncertainty, including aleatory variability and variation from effects not fully accounted for by σ_E or σ_S such as directivity. Thus, σ^{III} is comparable to the event-corrected, single-station standard deviation, ϕ_{SS}, of Rodriguez-Marek et al. (2011). In our results, values of σ^{III} are less than the values of ϕ_{SS} found by Rodriguez-Marek et al. (2011) for ground motions in the crust. This is likely because directivity in the model is mostly in one direction, and our station terms effectively remove most of the variability introduced by directivity. This leaves only deviations from the average directivity in σ^{III}, whereas variability due to directivity is still present in ϕ_{SS}. Another factor that could have caused our lower value of σ^{III} is the likely smaller aleatory variability of the more homogeneous foam model than found in the more heterogeneous earth; however, the difference between the σ^{III} and ϕ_{SS} variability are still most likely a result of the different analysis methods rather than differences between the model and the earth.

We found that the event terms contribute the most to the total variability, which means that most of the variability in the foam model is due to variations in the event magnitude. As with the aleatory variability discussed above, this is also an expected result since the path and station terms are so uniform in the model. Furthermore, our σ_E includes variability of event magnitudes; whereas GMPE variability τ does not contain variation due to differing magnitudes because τ is the between-event standard deviation for events with a given magnitude. Although our analysis separates the total variability into components, just as GMPEs do, the method in which these two total variabilities are decomposed does not allow for direct comparison of the components, and thus hinders our ability to compare the model and GMPE variabilities. However, it is remarkable that the total uncertainties from the foam rubber model are so similar to the values given by the NGAW2

GMPEs. This helps to justify the use of a physical model to study the variability in ground motions.

Since the peak ground motions in the model are not lognormally distributed, we reject our initial hypothesis that peak ground motions in the foam rubber model are lognormally distributed. We found that the greatest deviation of our empirical distribution from a lognormal distribution occurs near the median. This is in contrast with the findings of Restrepo-Velez and Bommer (2003) who found that, for GMPE residuals and earthquake-induced ground motions, the distributions deviate from lognormal only at the tails. Although there appears to be large deviations at the high tail in Figures 4 and 5, the deviations are within the 95% confidence limits, and thus statistically, the ground motions in the model are lognormal at the high tail. If the deviations from a lognormal distribution near the median in the model were also present in peak ground motions generated by earthquakes, this could cause a small but significant effect on seismic hazard estimates. For example, when we look at the horizontal distance between the lognormal distribution and the corresponding empirical distribution, in Figures 4 and 5, there is a greater increase in hazard where the horizontal distance is larger. In our dataset, the median of the residuals corresponds to exceedance levels commonly used in PSHA, and as already seen in the example at the end of the previous chapter, the empirical deviations from the lognormal distribution are significant enough to change hazard estimates by 15%. This is for a target hazard rate of 2% in fifty years, which is commonly used by engineers for strategic structures such as hospitals (Romeo and Prestininzi, 2000). A 15% increase in the hazard could affect the seismic design of buildings; although the factors-of-safety built in to the design are likely sufficient to accommodate this increase in hazard. For critical facilities such as nuclear power plants, where the high tail of the distribution is used to determine hazard corresponding to longer return periods, the deviation from lognormal is even greater, which would give a correspondingly larger increase in the hazard. If the shape of the model's empirical distribution were also seen in the distribution of ground motions from crustal earthquakes, then the current seismic designs for structures such hospitals and nuclear power plants could be insufficient.

In the foam model analysis, the deviation of the lognormal distribution from the empirical distribution increases, when compared to δ^I, after removing station means to produce δ^{II} and again after removing event means to produce δ^{III}. This is especially true for the larger ground motions represented in the high tail. However, moving to higher indexed residuals gives a corresponding decrease in the standard deviation; recall that $\sigma^I > \sigma^{II} > \sigma^{III}$. In a PSHA, we would use the larger σ^I value in the hazard integral when neither the magnitude nor the source-site distance are known, and we would use the smaller σ^{III} value when both the magnitude and the source-site distance

are known. For exceedance levels greater than the mean, a larger σ value (wider distribution) will increase the hazard. This is one of the reasons for the ongoing effort to find ways to lower the epistemic uncertainty in GMPEs (e.g. Abrahamson, 2006). Thus, it would seem that knowing the magnitude and distance, and being able to use the smaller σ^{III} value, which falls off faster for levels greater than the mean, would decrease the hazard. However, there is a trade-off between σ^{I} and σ^{III} that somewhat equalizes the two methods since knowledge of magnitude and distance changes the seismicity model, $n(\mathbf{x}, M)$, in the hazard integral. Thus, for a model-generated dataset, as with any other dataset, the epistemic uncertainty affects the hazard, and the only way to reduce the epistemic uncertainty is to further decompose the total uncertainty using improved analysis methods.

When we look at the PGA and PGV values generated by the ruptures in the foam, we see that they correlate with the measured stress drop. Brune's theoretical model (1970) suggests that particle velocity in the near field is proportional to the effective stress measured on the fault during a rupture. In the foam model, all stations are in the near field, but we can not assume that peak ground motion values in the far field stations would also be proportional to the stress drop. This is because of factors such as attenuation and geometrical spreading that reduce ground motion amplitudes at greater source-site distances and thus degrade the correlation of peak ground motions to stress drop at far field stations. Although we can't measure stress drop in the earth, the agreement of the foam rubber model with Brune's theoretical model provides some evidence in favor of the hypothesis that peak ground motions are correlated with stress drop.

Based on the results and conclusions of this study, future work is warranted. The model that provided the data for this analysis was built twenty years ago, and with the advances in material science, it may be possible to find a material that is more similar to rock in the areas of coefficient of friction and strain rate as well as in the brittle properties of rock such as surface roughness and fault gouge. It would also be good to build an apparatus that could simulate the higher pressures and heat found at seismogenic depths and also address characteristics such as fault healing. Although it would be ideal to create a physical model with these characteristics, it is important to recall that the foam rubber has significant advantages over a more advanced model: foam rubber is inexpensive, commonly available, light weight, and easy to work with while maintaining properties suitable for study of ground motions from stick-slip ruptures. Another improvement would be to decompose the data into parts in a manner similar to the method used in GMPEs. This would allow a direct comparison of the components of variability. Based on the results of this study and previous studies on the suitability of both logarithmic transformations and the lognormal distribution, it is

clear that further research on the distribution of peak ground motions in the earth and in physical models, along with the distribution of GMPE residuals, is justified. In particular, in future GMPE development, especially for projects that use a large dataset such as the NGAW2 GMPEs, finding the true distribution of ground motion amplitudes from the dataset would aid in understanding the behavior of repeating ruptures.